Protein Cell 2010, 1(6): 595–603
DOI 10.1007/s13238-010-0070-6

Protein & Cell

RESEARCH ARTICLE

Crystal structure of the C-terminal domain of the ε subunit of human translation initiation factor eIF2B

Jia Wei[1,2], Minze Jia[1], Cheng Zhang[1], Mingzhu Wang[1], Feng Gao[1], Hang Xu[1] ✉, Weimin Gong[1] ✉

[1] National Laboratory of Biomacromolecules, Institute of Biophysics, Chinese Academy of Sciences, Beijing 100101, China
[2] College of Life Sciences, Graduate University of Chinese Academy of Sciences, Beijing 100049, China
✉ Correspondence: wgong@ibp.ac.cn (W. Gong), hxu@moon.ibp.ac.cn (H. Xu)
Received April 30, 2010 Accepted May 25, 2010

ABSTRACT

Eukaryotic translation initiation factor eIF2B, the guanine nucleotide exchange factor (GEF) for eIF2, catalyzes conversion of eIF2·GDP to eIF2·GTP. The eIF2B is composed of five subunits, α, β, γ, δ and ε, within which the ε subunit is responsible for catalyzing the guanine exchange reaction. Here we present the crystal structure of the C-terminal domain of human eIF2Bε (eIF2Bε-CTD) at 2.0-Å resolution. The structure resembles a HEAT motif and three charge-rich areas on its surface can be identified. When compared to yeast eIF2Bε-CTD, one area involves highly conserved AA boxes while the other two are only partially conserved. In addition, the previously reported mutations in human eIF2Bε-CTD, which are related to the loss of the GEF activity and human VWM disease, have been discussed. Based on the structure, most of such mutations tend to destabilize the HEAT motif.

KEYWORDS eukaryotic translation initiation factor 2B (eIF2B), guanine nucleotide exchange factor (GEF), crystal structure, HEAT motif, vanishing white matter (VWM)

INTRODUCTION

The formation of the Met-tRNA$_i^{Met}$·eIF2·GTP ternary complex results in the 43S pre-initiation complex (PIC) and is essential for cap-dependent translation initiation in eukaryote (Kapp and Lorsch, 2004; Marintchev and Wagner, 2004; Sonenberg and Hinnebusch, 2007). Because this ternary complex formation requires GTP-bound eIF2, eIF2·GDP can not enter the initiation cycle until GDP is exchanged to GTP. Such exchange is catalyzed by eIF2B and known as one of the rate limiting steps in translation initiation (Pavitt, 2005). It has been found that even little disturbance in eIF2B function may cause severe problems. For example, mutations of eIF2B have been identified in an autosomal recessive neurodegenerative disease, known as VWM/CACH (vanishing white matter or childhood ataxia with central nervous system hypomyelination) (Li et al., 2004; Fogli and Boespflug-Tanguy, 2006; Scali et al., 2006; Maletkovic et al., 2008).

The eIF2B consists of five subunits α–ε, which can be divided to two subcomplexes according to their functions (Cigan et al., 1993; Pavitt et al., 1998; Williams et al., 2001a, b; Pavitt, 2005; Mohammad-Qureshi et al., 2007a). The subunits α, β and δ form a regulatory subcomplex, which responds to the phosphorylation of eIF2α and cellular stresses (Pavitt et al., 1998; Krishnamoorthy et al., 2001; Williams et al., 2001a; Dever, 2002; Hinnebusch, 2005; Smirnova et al., 2005). Another subcomplex is catalysis relevant, containing subunits γ and ε. The subunit ε is responsible for the guanine nucleotide exchange reaction, and can be regulated by direct phosphorylation (Wang et al., 2001; Wang and Proud, 2008). Interestingly, the C-terminal fragment of yeast eIF2Bε (residues 518–712) is sufficient to catalyze the guanine nucleotide exchange of eIF2 (Pavitt et al., 1998; Gomez et al., 2002; Mohammad-Qureshi et al., 2007b).

The eIF2Bε-CTD not only covers the minimal catalytic domain, but also contains highly conserved regions for interaction with other proteins. Two AA boxes (rich in acidic and aromatic residues) in eIF2Bε-CTD (Asano et al., 1999; Boesen et al., 2004) are also conserved in eIF5 and eIF4G (Marcotrigiano et al., 2001; Bieniossek et al., 2006; Wei et al.,

2006). eIF2Bε and eIF5 employ these AA boxes to bind lysine-rich K boxes in eIF2β (Das et al., 1997; Asano et al., 1999; Das and Maitra, 2000; Singh et al., 2006). In addition to the conserved sequence at AA boxes, similar structural folding known as HEAT motif is observed in the C-terminal domains of eIF2Bε, eIF5 and eIF4G.

In this study, the 2.0-Å crystal structure of the C-terminal domain (residues 547–721) of human eIF2Bε was determined, which has been the best model of human eIF2Bε-CTD with the highest resolution. The HEAT motif in this structure is similar to that in its yeast homolog, but they have low sequence identity and differ in the arrangement of their internal helices as well as in surface electrostatic potential. Finally, the reported mutations of human eIF2Bε-CTD related to catalytic activity and VWM/CACH are discussed based on the structure.

RESULTS

Overall structure

The crystal structure of human eIF2Bε-CTD has been solved at 2.0-Å resolution with MAD method and refined to R_{work} and R_{free} of 20.4% and 25.5%, respectively (Table 1). Similar to its homolog in yeast (PDB ID: 1PAQ) (Boesen et al., 2004), the human eIF2Bε-CTD structure is highly helical, containing nine α-helices (α1–9) and two 3_{10}-helices (η1 and η2) (Fig. 1). These helices are divided into four layers of helical repeats, each containing one anti-parallel helical pair. These helical pairs are packed along the axis that is perpendicular to the helices, while left-handed twisting occurs between adjacent layers. By such manner, human eIF2Bε-CTD is assembled into a globular domain with approximate dimensions of 45 × 40 × 30 $Å^3$, which is widely recognized as HEAT motif and has been reported to function in protein interactions (Marcotrigiano et al., 2001; Bieniossek et al., 2006; Wei et al., 2006). In addition, helices α6, α7 and α9 constitute two AA boxes (Fig. 2), which are highly conserved and required for the interaction with eIF2β N-terminal lysine-rich portion (Asano et al., 1999).

Structural comparison of the eIF2Bε-CTDs from human and yeast

Although the overall folding of human eIF2Bε-CTD is similar to that of yeast eIF2Bε-CTD (PDB ID: 1PAQ) (Boesen et al., 2004) (154 Cα's aligned with RMSD of 2.3 Å by using DALI) (Holm and Park, 2000), these domains exhibit different structural features due to their low sequence identity (20%). First, the bending angles in individual helices show significant variation in human and yeast eIF2Bε-CTD. An extreme example is demonstrated at the last helical repeat in human eIF2Bε-CTD, where the bending degree is so high that an extra helix (α8) is formed to adapt to such bending conformation (Fig. 1 and Fig. 2). In addition, the conformation of the loop linkage between α3 and α4 is quite different (Fig. 3A). The α3/η1 helix in human eIF2Bε-CTD terminates earlier than its yeast counterpart (α3) and thus releases two end residues into loop conformation (Fig. 2 and Fig. 3A). Finally, both eIF2Bε-CTD domains contain two 3_{10}-helices that form natural extension of the adjacent alpha helices. In human eIF2Bε-CTD, the first 3_{10}-helix (η1) is found at the C-terminus of α3 and the second (η2) is at the N terminus of α6. However, in yeast, the two 3_{10}-helices are accommodated at the C-terminus of α4 and at the N-terminus of α8, respectively (Fig. 2).

Surface property of human eIF2Bε-CTD

The surface of human eIF2Bε-CTD contains three areas with condensed charge, two acidic and one basic (Fig. 3B). The first area (area I) is acidic and formed by residues Glu591, Glu602, Glu644, Asp651, Glu655, Glu657, Asp689 and Asp692. Area II includes five acidic residues (Glu674, Glu678, Glu679, Glu712 and Glu714) and two aromatic residues (Tyr671 and Trp709), all of which are involved in the two AA boxes (Fig. 2 and Fig. 3B). Composed of Lys626, Lys665, Gln702 and Arg705, area III is positively charged and located at the opposite side to the area I. The results of sequence alignment of eukaryotic eIF2Bε-CTD's (Fig. 2) demonstrate: all the above areas and residues therein are highly conserved among mammalian species; area II is mostly conserved among all species, suggesting a common interaction mode between eIF2Bε AA boxes and eIF2β; area I and III are only of limited similarity (Fig. 2, Fig. 3B and 3C), likely to underlie various regulatory mechanisms.

DISCUSSION

Structural implication of the mutation causing the loss of the GEF activity of eIF2B

It has been reported that Glu577Ala mutant of human eIF2Bε displays less catalytic activity and exhibits reduced binding affinity for eIF2 (Wang and Proud, 2008). This is consistent with the hypothesis that the corresponding residue in yeast eIF2Bε, Glu569, is critical in interacting with eIF2γ and catalyzing GDP-GTP exchange (Mohammad-Qureshi et al., 2008; Wang and Proud, 2008). In human eIF2Bε-CTD, Glu577 participates in a hydrogen/salt bonding network with Thr560 and Arg563 (Fig. 4A). As residues Glu577, Thr560 and Arg563 are highly conserved (Fig. 2) and a similar bonding network was identified in yeast eIF2Bε-CTD (Fig. 4B), the interactions between these residues are likely to play an important role in eIF2Bε-catalyzed nucleotide exchange. One obvious consequence of the above interactions is the protection and stabilization of Glu577 in the absence of eIF2γ, while further investigation is required for

Table 1 Statistics of data reduction and structure refinement

data collection statistics				
MAD data collection	inflection	peak	remote	refinement
space group		$C222_1$		$C222_1$
unit cell parameters		a = 46.5 Å, b = 66.0 Å, c = 136.5 Å		a = 46.5 Å, b = 66.1 Å, c = 136.1 Å
wavelength (Å)	0.9796	0.9794	0.9600	0.9794
resolution range (Å)[a]	50–2.3 (2.38–2.30)	50–2.3 (2.38–2.30)	50–2.3 (2.38–2.30)	50–2.0 (2.07–2.00)
No. of total reflections	69,384	69,256	69,370	95,130
No. of unique reflections	9770	9770	9719	13,260
average redundancy	7.1 (6.8)	7.1 (6.8)	7.1 (7.2)	7.2 (7.4)
completeness (%)	99.6 (100.0)	99.6 (100.0)	99.5 (100.0)	90.6 (84.1)
R_{merge}[b]	0.057 (0.155)	0.072 (0.170)	0.062 (0.151)	0.070 (0.313)
$<I>/<\sigma(I)>$	34.8 (11.1)	28.2 (9.8)	31.3 (11.6)	24.1 (4.8)
refinement statistics				
space group			$C222_1$	
unit cell parameters			a = 46.5 Å, b = 66.1 Å, c = 136.1 Å	
R_{work}/R_{free} (%)[c]			20.4/25.5	
r.m.s.d. bond length (Å)			0.0095	
r.m.s.d. bond angle (°)			1.18	
No. of protein residues			174	
No. of water molecules			144	
No. of glycerol molecules			1	
average temperature factor (Å^2)				
protein main-chain atoms			24.4	
protein side-chain atoms			25.8	
water molecules			27.6	
glycerol molecule			17.8	
ramachandran plot (%)				
residues in most favored regions			97.5	
residues in additionally allowed regions			2.5	
residues in generously allowed regions			0	
residues in disallowed regions			0	

[a] Data for the highest resolution bin is in parentheses.

[b] $R_{merge} = \sum|Ii-Im|/\sum Ii$, where Ii is the intensity of the measured reflection and Im is the mean intensity of all symmetry-related reflections.

[c] $R_{work} = \sum| |F_{obs}|-|F_{calc}| |/\sum|F_{obs}|$, where F_{obs} and F_{calc} are observed and calculated structure factors, respectively. $R_{free} = \sum_T| |F_{obs}|-|F_{calc}| |/\sum_T|F_{obs}|$, where T denotes a test data set of about 5% of the total reflections randomly chosen and set aside prior to refinement.

thorough and better understanding.

Structural implication of the mutations causing the human disease VWM/CASH

Up to date, several mutations in human eIF2Bε-CTD (residues 547–721) have been assigned with VWM/CACH, including Pro604Ser, Leu605frameshift, Trp628Arg, Trp628stop, Ile649Thr, Glu650Lys, Lys665–Tyr671 deletion, and Ser610–Asp613 deletion (Fogli and Boespflug-Tanguy, 2006; Scali et al., 2006; Maletkovic et al., 2008; Wu et al., 2009).

Deletion of four residues Ser610–Asp613 in human eIF2Bε-CTD was recently reported in a Chinese VWM patient (Wu et al., 2009). These four residues are located on the loop between helices α3 and α4 (Fig. 4C), which displays different

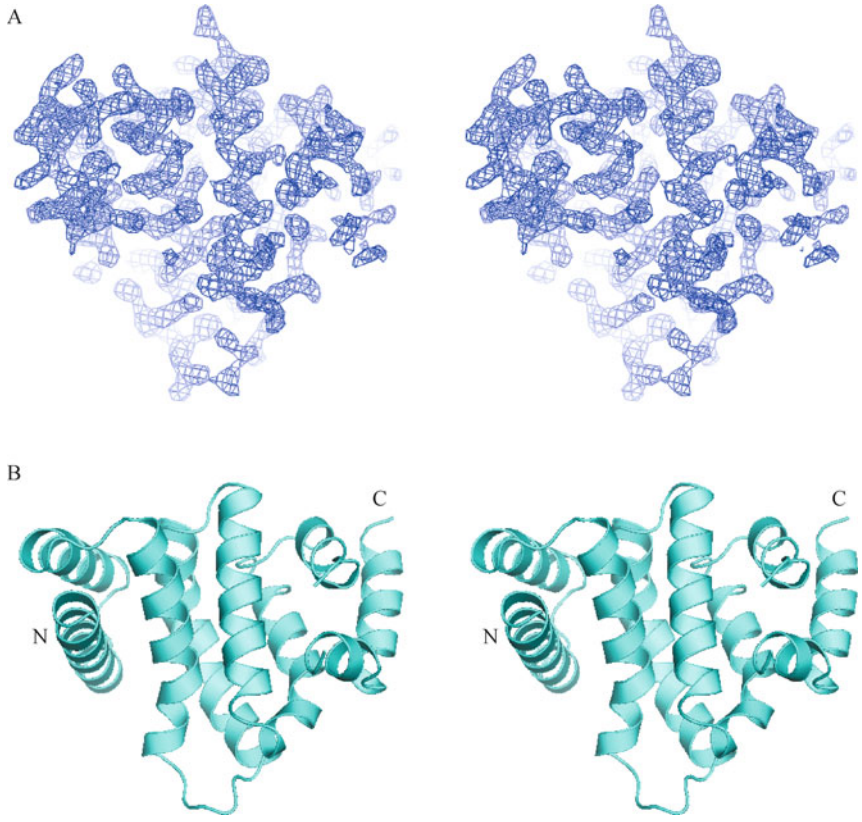

Figure 1. The overall structure of human eIF2Bε-CTD (stereo view). (A) Experimental electron density map based on the MAD phases after density modification (stereo view). The map is contoured at 1.5 σ. (B) Stereoview of the overall structure of human eIF2Bε-CTD.

conformations in human and yeast eIF2Bε-CTD as described above (Fig. 3A). With the loop shortened, the orientation of flanking helices α3/η1 and α4 might be forced to alter. This would consequently change the packing at the core of HEAT domain. In addition, this loop was suggested to play an important role in catalysis, based on the comparisons with other guanine nucleotide exchange factors (Boesen et al., 2004). Deletion of the residues Lys665–Tyr671 would highly reduce the stability of protein folding, since these residues are located in α6 (Fig. 4C), a core helix in HEAT repeat packing. Mutation of Trp628stop resulting in the lack of the two important AA boxes, as well as mutation of Leu605frameshift, would destroy the integral structure of eIF2Bε-CTD.

In the rest point mutations, Pro604Ser, Trp628Arg and Ile649Thr are identified in hydrophobic cores of human eIF2Bε-CTD. Residue Pro604 is involved in hydrophobic interactions with Tyr617, Leu621 and Leu624 (Fig. 4D), while Trp628 with Leu561, Phe603 and Leu624 (Fig. 4E), and Ile649 with Leu601, Leu646, Phe652, Phe653, Leu667, Phe670 and Leu676 (Fig. 4F). As polar residues were introduced by Pro604Ser, or Trp628Arg, or Ile649Thr, the hydrophobic interaction would be highly weakened. In contrast to the above three mutations, the environment around Glu650 is hydrophilic and it forms salt bond with Arg698 plus hydrogen bond with Trp684. These interactions stabilize the packing of helices α5, α8, α7 and the loop after α7 (Fig. 4G). Mutation of Glu650Lys would disturb such bonding network and therefore destabilize the HEAT folding.

Based on the above analysis, most VWM related mutations within human eIF2Bε-CTD are more likely to associate with structural integrity and stability, rather than the catalytic activity.

MATERIALS AND METHODS

Plasmid construction, protein expression and purification

The gene fragment of human eIF2Bε-CTD (residues 547–721) was amplified from a pDEST566 vector containing full-length eIF2Bε gene (a generous gift from Dr. James Zhijie Liu, Institute of Biophysics, Chinese Academy of Sciences), and constructed into p28 vector for expression. The above construct contained an incidental mutation Glu678Gly and N-terminal $(His)_6$ tag. The plasmid was transferred into methionine-auxotrophic *E. coli* strain b834 and cells were grown in M9 media containing 40 mg/L selenomethionine, 2 mM $MgSO_4$, 0.1 mM $CaCl_2$ and 0.05 μM $FeSO_4$, with kanamycin sulfate (50 μg/mL) at 37°C. Induction was performed by 0.25 mM IPTG for 3 h. Cells were lysed by sonication in 20 mM Tris-HCl, pH 7.7, 200 mM

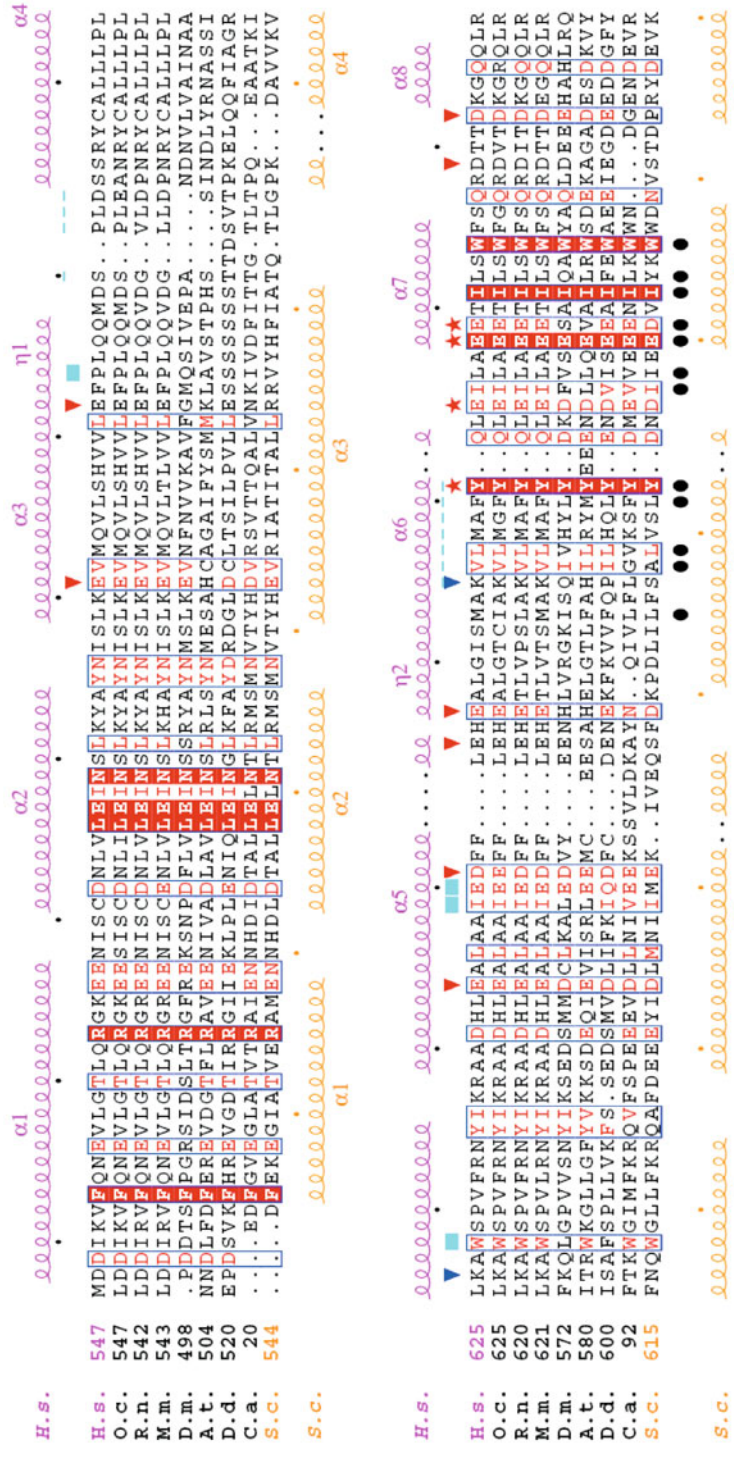

Figure 2. Multiple-sequence alignment of the C-terminal domains of eIF2Bε homologs. The α-helices and 3_{10}-helices in human and yeast eIF2Bε-CTD are denoted by the Greek characters α and η, respectively. Strictly conserved and similar residues are boxed and marked with red background and red letters, respectively. Filled and open circles denote residues in AA box 1 and 2, respectively. Red triangles, red asterisks and blue triangles represent residues involved in area I, II and III respectively. Cyan rectangles indicate the point mutation sites, while cyan dashed lines indicate deletions in VWM. Species abbreviation: H.s., *Homo sapiens*; O.c., *Oryctolagus cuniculus*; R.n., *Rattus norvegicus*; M.m., *Mus musculus*; C.e., *Caenorhabditis elegans*; D.m., *Drosophila melanogaster*; A.t., *Arabidopsis thaliana*; S.c., *Saccharomyces cerevisiae*. These amino acid sequences are aligned using the program ClustalW2 (Larkin et al., 2007), and the figure is prepared with ESPript (Gouet et al., 1999).

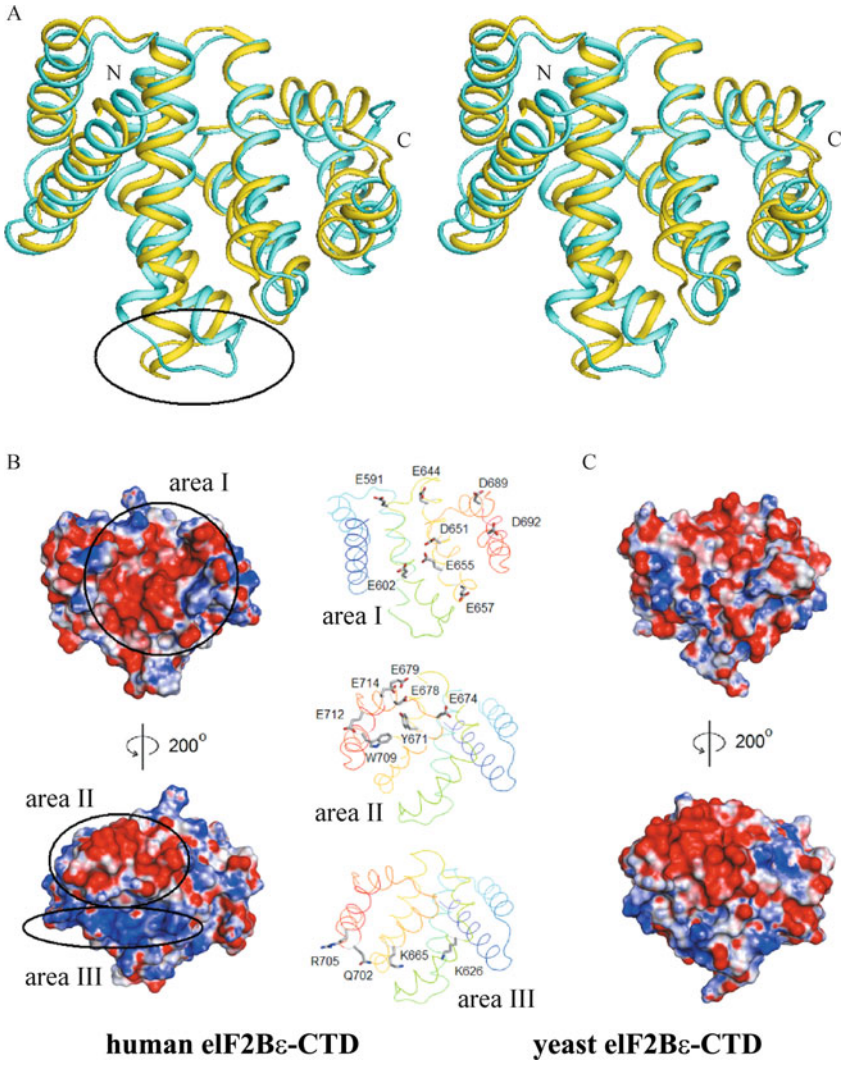

Figure 3. Structural comparison of human and yeast eIF2Bε-CTD. (A) Structural alignment of C-termini of human and yeast eIF2Bε (stereo view). Human and yeast eIF2Bε-CTD are shown in cyan and yellow, respectively. The loops with different conformation in two structures are circled. (B) Electrostatic potential distribution on the surface of human eIF2Bε-CTD in different views. Charge-rich areas I, II and III are circled. Residues involved in area I, II and III are demonstrated with their side chains, respectively. (C) Electrostatic potential distribution on the surface of yeast eIF2Bε-CTD (PDB ID: 1PAQ), shown as the same orientation in (B).

NaCl, 20 mM Imidazole, and 1 mM PMSF. The recombinant protein in lysate was purified by affinity chromatography with a Nickel Chelating Sepharose^{TM} Fast Flow column (GE), followed by gel filtration chromatography with a Superdex75 column (GE).

Crystallization and structure determination

Crystals of selenomethionyl human eIF2Bε-CTD were obtained by hanging-drop vapor-diffusion method plus streak-seeding using a feline whisker at 16°C within one week. Hanging drops were prepared by mixing a solution (1 μL) containing human eIF2Bε-CTD (19 mg/mL protein in 20 mM Tris-HCl, pH 7.7, 40 mM NaCl, 5 mM BME, and 0.2 mM EDTA) with 1 μL reservoir solution containing 15% PEG 8000, 0.2 M calcium acetate and 0.1 M sodium cocadylate. The crystals were flash frozen after soaking in reservoir solution supplemented with 15% (*w/v*) glycerol. A MAD data set at three different wavelengths ($\lambda_{inflection}$ = 0.9796 Å, λ_{peak} = 0.9794 Å, λ_{remote} = 0.9600 Å) was collected with a selenomethionyl human eIF2Bε-CTD crystal at 100 K on beamline X12C, NSLS, Brookhaven National Laboratory. A 2.0-Å resolution data set from another crystal was collected at wavelength 0.9794 Å for refinement at 100 K on beamline BL17U1 of Shanghai Synchrotron Radiation Facility. All the data were processed with HKL2000 (Otwinowski and Minor, 1997). The crystal belonged to the space group centered orthorhombic $C222_1$ and contained one human eIF2Bε-CTD molecule in the asymmetric unit (V_m = 2.47 Å^3 Da^{-1}, solvent content = 50.2%). Five of the six expected selenium atoms were located and used for phase determination at 2.3-Å by SOLVE (Terwilliger and Berendzen, 1999), and phases were

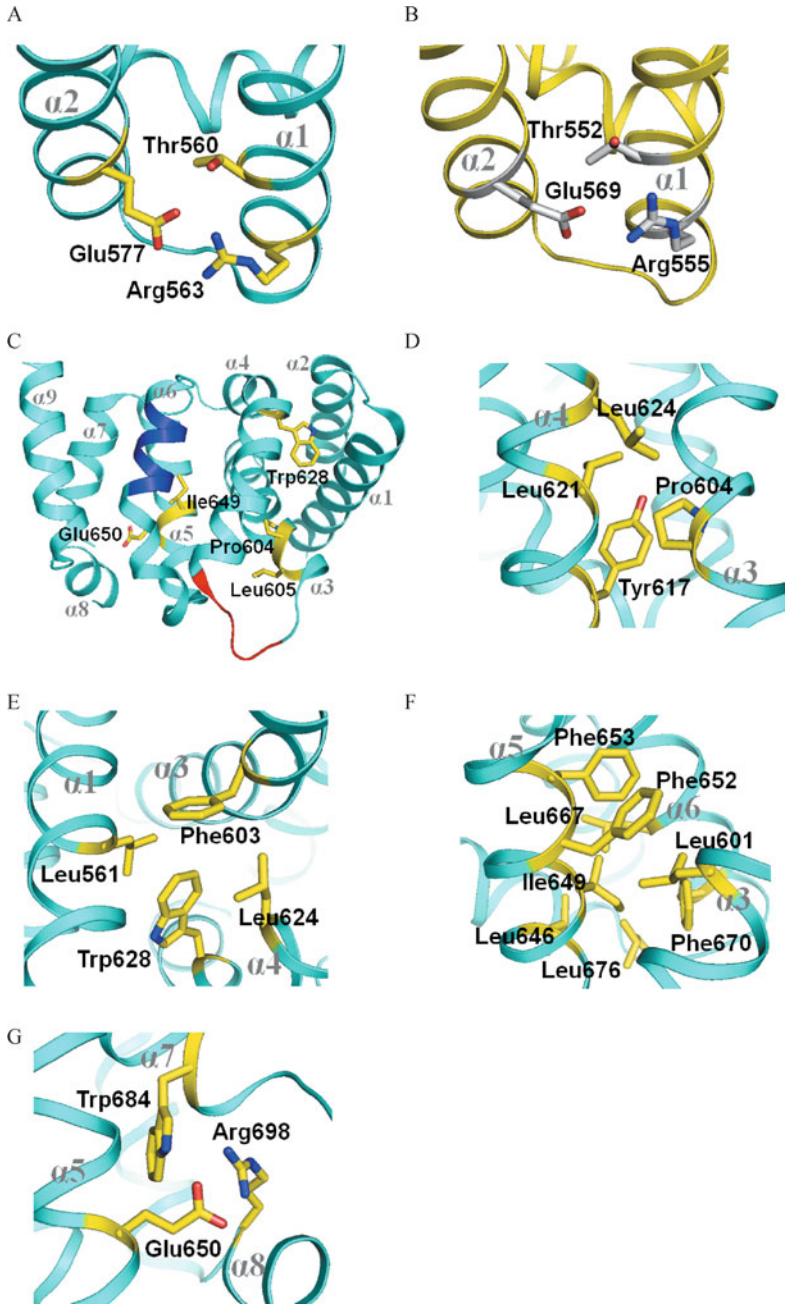

Figure 4. The critical residues of human eIF2Bε-CTD concerned with GEF activity of eIF2B and VWM/CACH disease. (A) Microenvironment around Glu577 in human eIF2Bε-CTD. (B) Microenvironment around Glu569 in yeast eIF2Bε-CTD. (C) Sites of mutations related to VWM disease are labeled on the structure of human eIF2Bε-CTD. Deletion sites of Ser610–Asp613Δ and Lys665–Tyr671Δ are colored red and blue, respectively. Other mutation sites at Pro604, Leu605, Trp628, Ile649 and Glu650 are labeled in yellow. (D) Hydrophobic contacts of Pro604 with surrounding residues Tyr617, Leu621 and Leu624. (E) Hydrophobic contacts of Trp628 with surrounding residues Leu561, Leu624 and Phe603. (F) Hydrophobic core formed by Ile649, Leu601, Leu652, Phe653, Leu667, Leu646, Leu676 and Phe670. (G) The ion pair and hydrogen bond formed by Glu650 with Arg698 and Trp684, respectively.

subsequently improved by density modification with RESOLVE (Terwilliger, 2000, 2003) for initial model building. The model was refined with 2.0-Å resolution data by Coot (Emsley and Cowtan, 2004), CNS (Brunger, 1998, 2007) and Refmac5 (Murshudov et al., 1997) for additional model building and adjustment. In the final model, the electron densities of residues Glu716–Asp721 were invisible and

those of Glu715, Thr690 and Thr691 were poor, so these 9 residues were excluded.

Structure modeling and analysis

In the experimental model, the incidental mutation Glu678Gly was located at the macromolecular surface. Therefore, it was expected to make the least impact on the 3-D folding of human eIF2Bε-CTD. To achieve a realistic distribution of electrostatic potential, structure modeling was performed to replace Gly678 by Glu, using Modeler (Sali and Blundell, 1993; Fiser et al., 2000; Martí-Renom et al., 2000; Eswar et al., 2006). As expected, only a limited change was observed in the adjusted model, where the side chain of Glu714 was slightly altered. Based on the adjusted structure, the surface electrostatic property was analyzed with APBS (Baker et al., 2001) and structural representations were generated using PyMOL [http://www.pymol.org].

COORDINATES DEPOSITION

The atomic coordinates and structural factors for human eIF2Bε-CTD have been deposited in the Protein Data Bank (PDB) with the accession code 3JUI.

ACKNOWLEDGEMENTS

The authors would like to thank Prof. Ruiming Xu in Institute of Biophysics, Chinese Academy of Sciences for MAD data collection at the National Synchrotron Light Source, Brookhaven National Laboratory (New York, USA). Other synchrotron-radiation experiments were performed at BL17U1 of Shanghai Synchrotron Radiation Facility (SSRF, Shanghai, China). This work was supported by the National Programs for High Technology Research and Development Program (863 Program) (Grant No. 2006AA02A316) and the National Basic Research Program (973 Program) (Grant Nos. 2004CB520801, 2006CB910903, 2007CB914304, 2009CB825501 and 2010CB912301) of the Ministry of Science and Technology, National Natural Science Foundation of China (Grant Nos. 30721003 and 30870484), and the Chinese Academy of Sciences (Grant No. KSCX2-YW-R61).

ABBREVIATIONS

eIF2B, eukaryotic translation initiation factor 2B; eIF2B-CTD, C-terminal domain of human eIF2B; GEF, guanine nucleotide exchange factor; PIC, pre-initiation complex; VWM, vanishing white matter; η1, the first 3_{10}-helix; η2, the second 3_{10}-helix

REFERENCES

Asano, K., Krishnamoorthy, T., Phan, L., Pavitt, G.D., and Hinnebusch, A.G. (1999). Conserved bipartite motifs in yeast eIF5 and eIF2Bepsilon, GTPase-activating and GDP-GTP exchange factors in translation initiation, mediate binding to their common substrate eIF2. EMBO J 18, 1673–1688.

Baker, N.A., Sept, D., Joseph, S., Holst, M.J., and McCammon, J.A. (2001). Electrostatics of nanosystems: application to microtubules and the ribosome. Proc Natl Acad Sci U S A 98, 10037–10041.

Bieniossek, C., Schütz, P., Bumann, M., Limacher, A., Uson, I., and Baumann, U. (2006). The crystal structure of the carboxy-terminal domain of human translation initiation factor eIF5. J Mol Biol 360, 457–465.

Boesen, T., Mohammad, S.S., Pavitt, G.D., and Andersen, G.R. (2004). Structure of the catalytic fragment of translation initiation factor 2B and identification of a critically important catalytic residue. J Biol Chem 279, 10584–10592.

Brunger, A.T. (2007). Version 1.2 of the Crystallography and NMR system. Nat Protoc 2, 2728–2733.

Brunger, A.T., Adams, P.D., Clore, G.M., DeLano, W.L., Gros, P., Grosse-Kunstleve, R.W., Jiang, J.S., Kuszewski, J., Nilges, M., Pannu, N.S., *et al*. (1998). Crystallography & NMR system: a new software suite for macromolecular structure determination. Acta Crystallogr 54, 905–921.

Cigan, A.M., Bushman, J.L., Boal, T.R., and Hinnebusch, A.G. (1993). A protein complex of translational regulators of GCN4 mRNA is the guanine nucleotide-exchange factor for translation initiation factor 2 in yeast. Proc Natl Acad Sci U S A 90, 5350–5354.

Das, S., Maiti, T., Das, K., and Maitra, U. (1997). Specific interaction of eukaryotic translation initiation factor 5 (eIF5) with the beta-subunit of eIF2. J Biol Chem 272, 31712–31718.

Das, S., and Maitra, U. (2000). Mutational analysis of mammalian translation initiation factor 5 (eIF5): role of interaction between the beta subunit of eIF2 and eIF5 in eIF5 function *in vitro* and *in vivo*. Mol Cell Biol 20, 3942–3950.

Dever, T.E. (2002). Gene-specific regulation by general translation factors. Cell 108, 545–556.

Emsley, P., and Cowtan, K. (2004). Coot: model-building tools for molecular graphics. Acta Crystallogr 60, 2126–2132.

Eswar, N., Webb, B., Marti-Renom, M.A., Madhusudhan, M.S., Eramian, D., Shen, M.Y., Pieper, U., and Sali, A. (2006). Comparative protein structure modeling using Modeller. Curr Protoc Bioinformatics Chapter 5, Unit 5.6.

Fiser, A., Do, R.K., and Sali, A. (2000). Modeling of loops in protein structures. Protein Sci 9, 1753–1773.

Fogli, A., and Boespflug-Tanguy, O. (2006). The large spectrum of eIF2B-related diseases. Biochem Soc Trans 34, 22–29.

Gomez, E., Mohammad, S.S., and Pavitt, G.D. (2002). Characterization of the minimal catalytic domain within eIF2B: the guanine-nucleotide exchange factor for translation initiation. EMBO J 21, 5292–5301.

Gouet, P., Courcelle, E., Stuart, D.I., and Métoz, F. (1999). ESPript: analysis of multiple sequence alignments in PostScript. Bioinformatics 15, 305–308.

Hinnebusch, A.G. (2005). Translational regulation of GCN4 and the general amino acid control of yeast. Annu Rev Microbiol 59, 407–450.

Holm, L., and Park, J. (2000). DaliLite workbench for protein structure comparison. Bioinformatics 16, 566–567.

Kapp, L.D., and Lorsch, J.R. (2004). The molecular mechanics of eukaryotic translation. Annu Rev Biochem 73, 657–704.

Krishnamoorthy, T., Pavitt, G.D., Zhang, F., Dever, T.E., and Hinnebusch, A.G. (2001). Tight binding of the phosphorylated alpha subunit of initiation factor 2 (eIF2alpha) to the regulatory subunits of guanine nucleotide exchange factor eIF2B is required for inhibition of translation initiation. Mol Cell Biol 21, 5018–5030.

Larkin, M.A., Blackshields, G., Brown, N.P., Chenna, R., McGettigan, P.A., McWilliam, H., Valentin, F., Wallace, I.M., Wilm, A., Lopez, R., *et al*. (2007). Clustal W and Clustal X version 2.0. Bioinformatics 23, 2947–2948.

Li, W., Wang, X., Van Der Knaap, M.S., and Proud, C.G. (2004). Mutations linked to leukoencephalopathy with vanishing white matter impair the function of the eukaryotic initiation factor 2B complex in diverse ways. Mol Cell Biol 24, 3295–3306.

Maletkovic, J., Schiffmann, R., Gorospe, J.R., Gordon, E.S., Mintz, M., Hoffman, E.P., Alper, G., Lynch, D.R., Singhal, B.S., Harding, C., *et al*. (2008). Genetic and clinical heterogeneity in eIF2B-related disorder. J Child Neurol 23, 205–215.

Marcotrigiano, J., Lomakin, I.B., Sonenberg, N., Pestova, T.V., Hellen, C.U., and Burley, S.K. (2001). A conserved HEAT domain within eIF4G directs assembly of the translation initiation machinery. Mol Cell 7, 193–203.

Marintchev, A., and Wagner, G. (2004). Translation initiation: structures, mechanisms and evolution. Q Rev Biophys 37, 197–284.

Martí-Renom, M.A., Stuart, A.C., Fiser, A., Sánchez, R., Melo, F., and Sali, A. (2000). Comparative protein structure modeling of genes and genomes. Annu Rev Biophys Biomol Struct 29, 291–325.

Mohammad-Qureshi, S.S., Haddad, R., Hemingway, E.J., Richardson, J.P., and Pavitt, G.D. (2007a). Critical contacts between the eukaryotic initiation factor 2B (eIF2B) catalytic domain and both eIF2beta and-2gamma mediate guanine nucleotide exchange. Mol Cell Biol 27, 5225–5234.

Mohammad-Qureshi, S.S., Haddad, R., Palmer, K.S., Richardson, J. P., Gomez, E., and Pavitt, G.D. (2007b). Purification of FLAG-tagged eukaryotic initiation factor 2B complexes, subcomplexes, and fragments from Saccharomyces cerevisiae. Methods Enzymol 431, 1–13.

Mohammad-Qureshi, S.S., Jennings, M.D., and Pavitt, G.D. (2008). Clues to the mechanism of action of eIF2B, the guanine-nucleotide-exchange factor for translation initiation. Biochem Soc Trans 36, 658–664.

Murshudov, G.N., Vagin, A.A., and Dodson, E.J. (1997). Refinement of macromolecular structures by the maximum-likelihood method. Acta Crystallogr 53, 240–255.

Otwinowski, Z., and Minor, W. (1997). Processing of X-ray diffraction data collected in oscillation mode. Methods Enzymol 276, 307–326.

Pavitt, G.D. (2005). eIF2B, a mediator of general and gene-specific translational control. Biochem Soc Trans 33, 1487–1492.

Pavitt, G.D., Ramaiah, K.V., Kimball, S.R., and Hinnebusch, A.G. (1998). eIF2 independently binds two distinct eIF2B subcomplexes that catalyze and regulate guanine-nucleotide exchange. Genes Dev 12, 514–526.

Sali, A., and Blundell, T.L. (1993). Comparative protein modelling by satisfaction of spatial restraints. J Mol Biol 234, 779–815.

Scali, O., Di Perri, C., and Federico, A. (2006). The spectrum of mutations for the diagnosis of vanishing white matter disease. Neurol Sci 27, 271–277.

Singh, C.R., Lee, B., Udagawa, T., Mohammad-Qureshi, S.S., Yamamoto, Y., Pavitt, G.D., and Asano, K. (2006). An eIF5/eIF2 complex antagonizes guanine nucleotide exchange by eIF2B during translation initiation. EMBO J 25, 4537–4546.

Smirnova, J.B., Selley, J.N., Sanchez-Cabo, F., Carroll, K., Eddy, A. A., McCarthy, J.E., Hubbard, S.J., Pavitt, G.D., Grant, C.M., and Ashe, M.P. (2005). Global gene expression profiling reveals widespread yet distinctive translational responses to different eukaryotic translation initiation factor 2B-targeting stress pathways. Mol Cell Biol 25, 9340–9349.

Sonenberg, N., and Hinnebusch, A.G. (2007). New modes of translational control in development, behavior, and disease. Mol Cell 28, 721–729.

Terwilliger, T.C. (2000). Maximum-likelihood density modification. Acta Crystallogr 56, 965–972.

Terwilliger, T.C. (2003). Automated main-chain model building by template matching and iterative fragment extension. Acta Crystallogr 59, 38–44.

Terwilliger, T.C., and Berendzen, J. (1999). Automated MAD and MIR structure solution. Acta Crystallogr 55, 849–861.

Wang, X., Paulin, F.E., Campbell, L.E., Gomez, E., O'Brien, K., Morrice, N., and Proud, C.G. (2001). Eukaryotic initiation factor 2B: identification of multiple phosphorylation sites in the epsilon-subunit and their functions *in vivo*. EMBO J 20, 4349–4359.

Wang, X., and Proud, C.G. (2008). A novel mechanism for the control of translation initiation by amino acids, mediated by phosphorylation of eukaryotic initiation factor 2B. Mol Cell Biol 28, 1429–1442.

Wei, Z., Xue, Y., Xu, H., and Gong, W. (2006). Crystal structure of the C-terminal domain of S.cerevisiae eIF5. J Mol Biol 359, 1–9.

Williams, D.D., Pavitt, G.D., and Proud, C.G. (2001a). Characterization of the initiation factor eIF2B and its regulation in Drosophila melanogaster. J Biol Chem 276, 3733–3742.

Williams, D.D., Price, N.T., Loughlin, A.J., and Proud, C.G. (2001b). Characterization of the mammalian initiation factor eIF2B complex as a GDP dissociation stimulator protein. J Biol Chem 276, 24697–24703.

Wu, Y., Pan, Y., Du, L., Wang, J., Gu, Q., Gao, Z., Li, J., Leng, X., Qin, J., Wu, X., *et al*. (2009). Identification of novel EIF2B mutations in Chinese patients with vanishing white matter disease. J Hum Genet 54, 74–77.

